Nanoscale Advances

ROYAL SOCIETY OF CHEMISTRY

PAPER

View Article Online
View Journal | View Issue

Cite this: *Nanoscale Adv.*, 2023, **5**, 5974

Green synthesis of fluorescent carbon nanodots from sage leaves for selective anticancer activity on 2D liver cancer cells and 3D multicellular tumor spheroids

Shadi Sawalha, *[a] Samer Abdallah, [b] Amal Barham,[a] Hala Badawi,[a] Zeina Barham,[a] Ahmad Ghareeb,[c] Giuseppe Misia,[d] Silvia Collavini,[e] Alessandro Silvestri,[f] Maurizio Prato [de] and Mohyeddin Assali *[c]

Carbon nanodots, a family of carbon-based nanomaterials, have been synthesized through different methods from various resources, affecting the properties of the resulting product and their application. Herein, carbon nanodots (CNDs) were synthesized with a green and simple hydrothermal method from sage leaves at 200 °C for 6 hours. The obtained CNDs are well dispersed in water with a negative surface charge (ζ-potential = −11 mV) and an average particle size of 3.6 nm. The synthesized CNDs showed concentration-dependent anticancer activity toward liver cancer (Hep3B) cell lines and decreased the viability of the cancer cells to 23% at the highest used concentration (250 μg ml^{-1} of CNDs). More interestingly, the cytotoxicity of the CNDs was tested in normal liver cell lines (LX2) revealed that the CNDs at all tested concentrations didn't affect their viability including at the highest concentration showing a viability of 86.7%. The cellular uptake mechanisms of CNDs were investigated and they are thought to be through energy-dependent endocytosis and also through passive diffusion. The main mechanisms of endocytosis were lipid and caveolae-mediated endocytosis. In addition, the CNDs have hindered the formation of 3D spheroids from the Hep3B hepatocellular carcinoma cell line. Hence, it would be concluded that the synthesized CNDs from sage are more highly selective to liver cancer cells than normal ones. The CNDs' cancer-killing ability would be referred to as the production of reactive oxygen species.

Received 23rd April 2023
Accepted 17th September 2023

DOI: 10.1039/d3na00269a

rsc.li/nanoscale-advances

1. Introduction

Cancer is one of the primary health issues affecting the global population and the second largest cause of death after cardiovascular disease. Despite recent substantial advancements in cancer treatment, aggressive tumors such as those of the lung, breast, pancreatic, and liver still cause significantly low patient survival rates.[1]

In the treatment of cancer, the methods currently used, such as chemotherapy and radiation therapy, destroy healthy cells and harm the body's production of new cells at the same time as killing cancer cells, and they are drawn-out procedures.[2] The chemotherapy currently in use lacks selectivity and affinities to particular malignancies. Recently, a few focused therapies have been created. However, they are pricey and only effective for specific cancers.[3]

Because of the damage caused by the current treatment used, researchers resorted to the use of targeted cancer therapy based on nanomaterials taking advantage of enhanced permeability and retention phenomena and the overexpression of specific receptors in cancer cells.[4,5] One of these well-developed nanomaterials is carbon-based nanomaterials such as carbon nanotubes (CNTs),[6,7] graphene,[8] and carbon nanodots (CNDs).[9]

CNDs used in cancer theranostics have been documented over the past ten years.[10] Numerous studies specifically examined the potential use of CNDs as targeted anticancer drug delivery systems.[11] Furthermore, the eradication of cancer cells has been achieved by CNDs through either photothermal therapy (PTT) or photodynamic therapy (PDT).[12]

[a]*Chemical Engineering Program, Faculty of Engineering and Information Technology, An-Najah National University, P.O. Box 7, Nablus, Palestine. E-mail: sh.sawalha@najah.edu*

[b]*Department of Biology and Biotechnology, Faculty of Science, An-Najah National University, P.O. Box 7, Nablus, Palestine*

[c]*Department of Pharmacy, Faculty of Medicine and Health Sciences, An-Najah National University, P.O. Box 7, Nablus, Palestine. E-mail: m.d.assali@najah.edu*

[d]*Department of Chemical and Pharmaceutical Sciences INSTM UdR Trieste, University of Trieste, via Licio Giorgieri 1, 34127 Trieste, Italy*

[e]*Center for Cooperative Research in Biomaterials (CIC BiomaGUNE), Basque Research and Technology Alliance (BRTA), Donostia-San Sebastián 20014, Spain*

[f]*Department of Molecular Sciences and Nanosystems, Ca' Foscari University of Venice, Venezia 30170, Italy*

CNDs were discovered as a result of the purification of the single-walled carbon nanotube (SWNT) process in 2004 and became an important and interesting topic in nanomaterial and cancer therapy.[13]

"Top-down" and "bottom-up" synthesis are the two main categories of synthetic techniques used to create CNDs. The "top-down" approach is used to synthesize CNDs typically by breaking down carbon–carbon bonds of large molecules existing in bulk carbon materials such as charcoal, graphite, fullerene, *etc.*[14] This can be achieved by different methods such as electrochemical exfoliation,[15] laser ablation,[16] and arc discharge.[17] In "bottom-up", methods such as microwave-assisted polymerization, pyrolysis,[18–23] hydrothermal/solvothermal,[24] and carbonization are used to convert small organic molecules contained in the precursor to carbon nanodots.[25–27]

CNDs have been synthesized from various resources, such as man-made[28–31] and natural resources,[32–36] and they have also been synthesized from various herbs and plants and have been used in different biomedical applications.[37,38]

One of the reasons that make CNDs good candidates for medical applications, especially as an anticancer agent, is their properties that caught and attracted the researcher's attention such as biocompatibility,[39] water dispersibility,[40] cytotoxicity,[41] good conductivity,[42] quantum yield and small size,[43] and fluorescence emission.[44]

CNDs as anticancer agents have been studied by different researchers to treat a wide variety of cancer types such as breast cancer which has been treated by CNDs synthesized from bamboo.[45] However, there have not been many studies on liver cancer. Chi-Lin Li *et al.* prepared CNDs from extracted ginger juice and used them to kill liver cancer cells (HepG2), where 50% of the cancer cells were killed at a concentration of 350 μg ml^{-1}.[46]

In this research and for the first time (to the best of our knowledge) CNDs have been synthesized from sage leaves with a green hydrothermal method and characterized as being used as an anticancer agent for liver cancer cells (Hep3B) and performing cell viability tests for normal liver cells, to investigate the CND selectivity toward cancer cells. In addition, CNDs' effect on prohibiting 3D spheroid formation has been investigated. Finally, the possible mechanism of anticancer activity has been studied.

2. Materials and methods

Fresh sage leaves as the precursor for carbon nanodot synthesis were obtained from the local market. All used chemicals and reagents were purchased from Sigma-Aldrich and used without any further purification. Distilled water was the media used in the synthesis of CNDs.

A Beckman Coulter DU 800 spectrophotometer collects the absorption of UV-Vis spectra between 200 and 800 nm. A PerkinElmer LS50B fluorescence spectrophotometer was used to measure the steady-state fluorescence in the emission range of 320 to 650 nm. Fluorescence spectra values were collected at excitation wavelengths ranging from 300 to 440 nm with a 20 nm increment. A Thermo Scientific Nicolet IS5 FTIR system equipped with an ATR sampling apparatus, 64 scans at 8 cm^{-1} resolution were used to record the Fourier transform infrared (FT-IR) spectra of synthesized CNDs in the range of 4000–650 cm^{-1}. Atomic force microscopy (AFM) images and profiles were captured using a Nanosurf Core AFM microscope and the images were analyzed using Gwyddion software. The samples were prepared by drop-casting CND diluted solution on mica substrates and then vacuum drying at 120 °C. By utilizing Nano Brook Omni equipment using phase analysis light scattering (PALS), ζ-potential measurements were performed. Transmission electron microscope (TEM) images were obtained using a JEOL JEM 1400-Plus microscope with a Gatan US1000 CCD camera and 120 kV accelerating voltage; samples were prepared by drop-casting diluted CND solutions on lacey carbon film-covered copper TEM grids. X-ray photoelectron spectroscopy (XPS) measurements were conducted using a PHI 5000 VersaProbe III photoelectron spectrometer. For XPS samples, CND solutions were drop cast on a gold substrate and dried under vacuum for 24 h.

2.1. Synthesis of CNDs

By a green hydrothermal method, CNDs were synthesized utilizing fresh sage leaves. First, sage leaves were washed well with water and then dried to remove excess water. 0.5 grams of sage leaves were cut into small pieces and then dispersed in 50 ml of distilled water. The mixture was inserted into a Teflon-lined stainless-steel autoclave and then heated to 200 °C for 6 h; subsequently, the autoclave was cooled down to room temperature, and the solution was centrifuged for 10 minutes at 3500 rpm. The resulting supernatant was filtered through a 0.45 μm microfilter. The formed CND solution was purified using a Sephadex 25-G size exclusion column. CND powder was obtained by freeze-drying the solution for 36 h and stored in the dark for further characterization and application.

2.2. Cancer activity and cytotoxicity

We analyzed the cytotoxicity of prepared CNDs on human hepatocellular carcinoma cell line (Hep3B) cells purchased from ATCC (HB-8064) and normal liver cells (LX2) purchased from Sigma-Aldrich (SCC064).

The first step in cell culture was culturing the cell line in T-175 cell culture flasks containing Roswell Park Memorial Institute (RPMI) basal medium supplemented with L-glutamine (1%), fetal bovine serum FBS (10%), and penicillin/streptomycin (1%). At 37 °C and 99% humidity, the cells were kept in a standard cell culture incubator at 5% CO_2 equipped with a UV-Vis lamp. The medium was removed and washed with Ca^{2+}-free phosphate buffer solution (PBS) before subculturing. Following that, cells were incubated in the incubator with 0.025% trypsin for up to 5 minutes until sufficient cells detached. Then, complete growth medium (CGM) was used to inactivate the trypsin, then the cell suspension was collected, and a trypan blue stain was used to determine the viable cell count before adjusting the cell concentration to 79 000 and 31 000 for HeP3B and LX2 cells respectively. In a 96-well plate, the

cells were seeded at 5000 cells per well. The cells were then allowed to adhere and accommodate overnight before tests were conducted. After 24 hours, we prepared different concentrations of CNDs which are 250 μg ml^{-1}, 200 μg ml^{-1}, 150 μg ml^{-1}, 100 μg ml^{-1}, and 50 μg ml^{-1} under 7.4 pH conditions. After that, we add 100 μl of each concentration per well. After 48 hours, 20 μl of MTS reagent was added to each well and incubated for 2 hours in the incubator. After that time, the absorbance was measured at 490 nm by using a plate reader.

2.3. Cellular uptake study of the synthesized carbon nanodots

To investigate the cellular uptake mechanism of the CNDs, Hep3B cells were seeded in a 96 well plate at 5000 cells per well and maintained at 4 °C or incubated with one of the various endocytosis inhibitors (NaN_3 10 mM, methyl-β-cyclodextrin 5 mg ml^{-1} (MβCD), chlorpromazine 10 μM (CPZ), genistein 200 μM, and amiloride 200 μM) for 1 h at 37 °C. The concentrations used are according to the literature.[47,48] After that, 100 μl of 200 μg ml^{-1} CNDs was added to each well. After that, an MTS assay was performed.

2.4. Capacity testing of 3D tumor spheroid formation

Human Hep3B liver cancer cells were cultured (4×10^3 cells) in ultra-low attachment 96-well plates in the presence of 150 μg ml^{-1} of carbon nanodots for 24 hours. Images of spheroids were captured 24 hours after incubation at a final magnification of 40× of an inverted microscope. ImageJ software was employed for analyzing images and their measurements.

2.5. Glutathione deficiency test

A glutathione deficiency test was carried out to investigate the ability of synthesized CNDs to generate reactive oxygen species (ROS). 0.8 mM of glutathione (GSH) was prepared in 50 mM bicarbonate buffer with a pH of 8.6. The positive control was 0.8 mM of GSH solution with 1 mM H_2O_2, and the negative control was set using a GSH solution. 255 μl of synthesized CNDs was dispersed separately in the bicarbonate buffer with GSH. All samples were conducted in duplicate and wrapped with aluminum foil. The samples were agitated in a shaker for 2 h with a speed of 250 rpm. After that, 15 μl of 100 mM DNTB Ellman's reagent and 780 μl of prepared 0.05 M Tris-HCl were added to each sample and measured its absorbance at wavelength $\lambda = 412$ nm.

3. Results and discussion

3.1. Synthesis and characterization

The bottom-up approach was followed up for the synthesis of CNDs from sage leaves, with the hydrothermal process at 200 °C for 6 hours. It is thought that the containing sage essential oils such as α-thujone, 1,8-cineole, and camphor[49] would be polymerized during hydrothermal forming aromatic clusters, and when their concentration reaches a critical supersaturation point, burnt nucleation takes place, in addition to carbonization occurring for organic contents to form carbon dots.[50] After

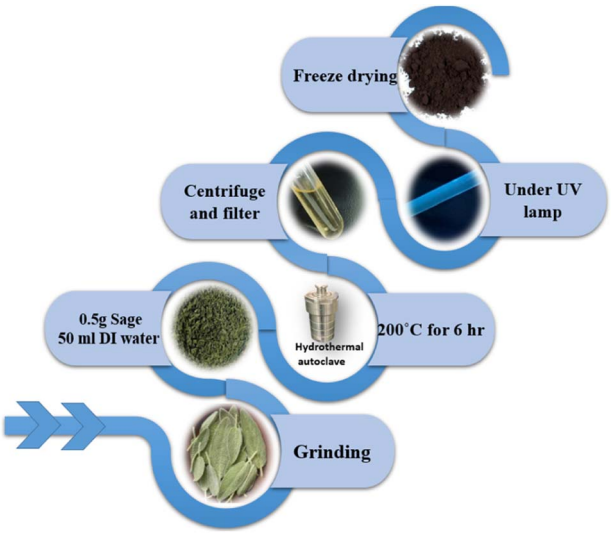

Fig. 1 Synthetic steps to prepare CNDs from sage leaves.

the synthesis of the CNDs, we conducted various purification procedures to remove any intermediate or precursor materials. In this process, we performed centrifugation, filtration, and most importantly column chromatography separation using a Sephadex G-25 which confirms the purification of the carbon nanodots. The synthesized CNDs have been obtained with a 15% product yield. Fig. 1 illustrates the synthesis process.

The morphology and size of synthesized carbon nanoparticles (CNDs) were characterized by using AFM and TEM microscopies. The CND height was measured to be in the range of 1–9 nm with an average of (3.6 ± 1.5 nm) as shown by the AFM results in Fig. 2a–c. On the other hand, the TEM micrograph (Fig. 2d & e) represents well-distributed particles with a size ranging from 2–7 nm with an average of 3.8 ± 1.6 nm. Both the AFM and TEM results would confirm that the formed CNDs are quasi-spherical in their shape and they are well-dispersed in the CND solution.

The chemical composition and surface functional groups were acquired by FTIR and XPS as shown in Fig. 3. The FTIR spectrum demonstrates different peaks at 3390, 3088, 2920,

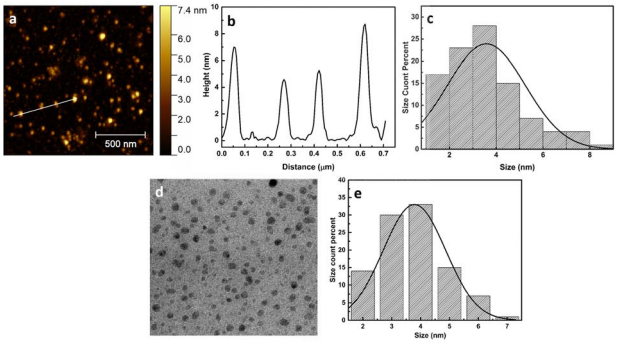

Fig. 2 (a) AFM image, (b) height profile, and (c) size distribution histogram extracted from AFM images of the prepared CND sample, (d) TEM image, and (e) size distribution histogram extracted from TEM images of the prepared CNDs.

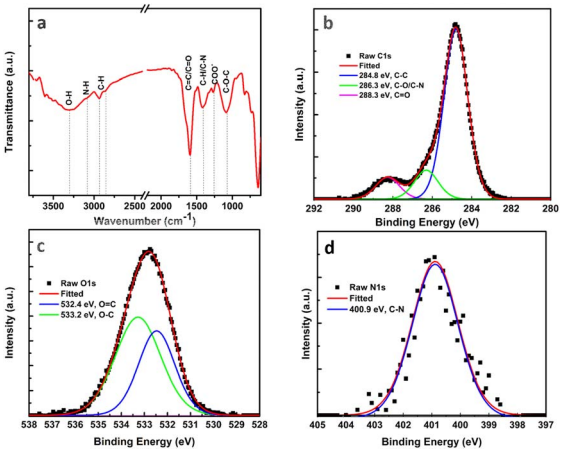

Fig. 3 (a) FTIR spectrum of the synthesized CNDs, (b) high-resolution C 1s XPS spectra, (c) high-resolution O 1s XPS spectra, and (d) high-resolution N 1s XPS spectra.

2860, 1600, 1417, 1259, and 1084, which could be related to O–H, N–H, C–H, C=C/C=O, C–N, COO–, and C–O–C bands respectively as shown in Fig. 3a.[51–54] The XPS measurement showed that the synthesized CNDs are composed of carbon, oxygen, and nitrogen elements with an atomic percent of 53.7, 44.1, and 2.2, respectively. The deconvolution of the high-resolution C 1s core (Fig. 3b) leads to three peaks at 284.8, 286.3, and 288.3 eV which can be related to C–C/C=C, C–O/C–N, and C=O functional groups respectively.[55,56] Besides that, the O 1s can be deconvoluted into two peaks of O=C at 532.4 eV and O–C at 533.2 eV as shown in Fig. 3c.[57] Finally, the nitrogen content is represented by the C–N functional group at 400.9 eV (Fig. 3d).[58] The XPS results are well-matched with those of FT-IR emphasizing the existence of varied oxygen groups on the surface of the synthesized CNDs such as hydroxyl, carbonyl, and carboxylic groups. The existence of highly oxygenated groups would confirm the stability and water solubility of synthesized particles,[59] in addition to the surface negative charge measured as PALS ζ-potential equal -11 ± 1.2 mV in phosphate buffer solution at (PBS @ PH $\approx$ 7.4).[60] The obtained ζ-potential is nearly similar to those obtained by other researchers, for example, CNDs synthesized from ascorbic acid by the hydrothermal method have a negative charge of −23 mV.[61] While CNDs from bovine gelatine gave a ζ-potential equal to −20 mV,[62] on the other hand, carbon dots from bamboo showed a ζ-potential equal to −4.78 mV.[63]

To investigate the optical characteristics of the synthesized CNDs, UV-Vis and photoluminescence spectral data were recorded. Under daylight, the synthesized CNDs are light yellow and tend to be transparent, but under UV light their color was blue. The UV-Vis spectrum exhibits strong absorption in the UV range with a tail extending to the visible region, as shown in Fig. 4a. The spectrum shows an absorption peak at 203 nm (shoulder) that is attributed to π–π* of the aromatic sp^2 hybridized carbon core;[64] besides that, two peaks at 280 nm and 360 nm are shown in the inset of Fig. 4a, which are ascribed to n–π* that is related to the existence of C=O and N=O bands.[65]

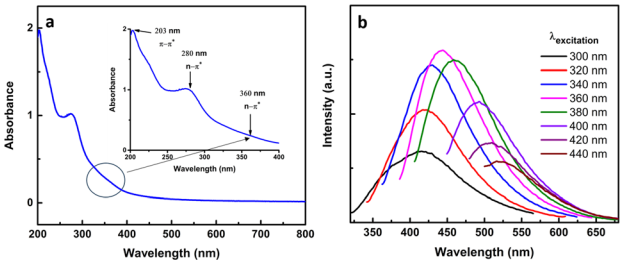

Fig. 4 (a) The UV-Vis absorption spectrum of the prepared CNDs (inset figure highlights the characteristic bands of CNDs), and (b) photoluminescence (PL) spectra of the prepared CNDs at different excitation wavelengths.

The fluorescence of synthesized CNDs was measured at different excitation wavelengths from 300–440 nm as shown in Fig. 4b. The CNDs gave a maximum emission of 443 nm when excited λ_{ex} equals 360 nm. When the excitation increased above 360 nm the CNDs exhibited a red shift with a decay of the fluorescence. This behavior of CND fluorescence is a well-known phenomenon,[66] and the photoluminescence of CNDs could be related to surface emission traps, surface defects, and surface functional groups.[67]

The quantum yield of CNDs was estimated @360 nm based on quinine sulfate (QY = 55%) as a reference using eqn (1).

$$\mathrm{QY} = Q_R \times \frac{I}{I_R} \times \frac{A_R}{A} \times \frac{I}{{n_R}^2} \quad (1)$$

QY is the quantum yield, I is the estimated integrated emission intensity, A is the absorption of the sample, and n is the refractive index. R refers to the reference fluorophore (quinine sulfate dissolved in 0.1 M H_2SO_4) of known quantum yield. n is equal to 1.33 for water.[68] The quantum yield was 1.95%.

Moreover, the stability of the prepared CNDs was examined for four months in the dark, and no precipitation or aggregations were formed. Furthermore, the fluorescence at 360 nm

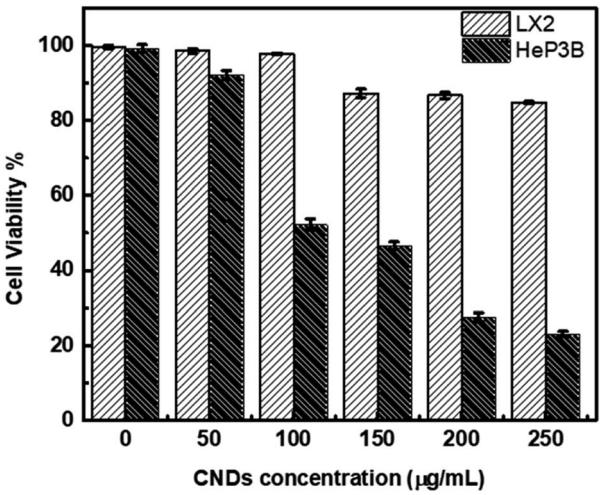

Fig. 5 Viability of Hep3B and LX2 cells after incubation with different concentrations of CNDs.

was examined weekly and the quantum yield (% QY) was estimated to be only a drop of about 6% (from 1.95 to 1.83%).

3.2. Cytotoxicity on Hep3B and LX2 cells

The cytotoxicity of the synthesized CNDs was tested against liver cancer cells (Hep3B) and normal liver cells (LX2) under exposure to light during the whole treatment process. The viability test was conducted to estimate the toxicity and efficiency of CNDs with selective targeting of the cancer cells.

The results showed that the synthesized CNDs were active as an anticancer therapeutic agent in destroying cancer cells (Hep3B) at different concentrations, while the normal liver cells (LX2) remained unaffected with an availability of more than 86.7%. This means that these CNDs show selectivity to the liver cancer cells.

Human hepatocellular carcinoma cell line (Hep3B) and normal liver cells (LX2) were treated with CNDs at concentrations of 50–250 μg ml^{-1}. As shown in Fig. 5 the Hep3B cell viability decreased with an increasing concentration to reach 23% at concentration 250 μg ml^{-1}. At the same time the normal cell LX2 viability decreased slightly to reach 86.7% at the same highest concentration. The IC_{50} value of the CNDs on Hep3B cells was 100 μg ml^{-1} whereas at that concentration the LX2 cells have 97.8% cell viability. This means that our CNDs have a selective effect on the cancer cells without affecting the normal liver cells.

3.3. Cellular uptake study of the CNDs

The possible mechanism of the cellular uptake of the CNDs could be an energy-dependent or energy-independent pathway.[69] The cytotoxicity of CNDs was determined after the incubation of the Hep3B cells at 4 °C or with sodium azide at 37 °C to examine the effect of temperature and ATP on the uptake process. As shown in Fig. 6, the cytotoxicity of the CNDs was reduced significantly in both cases which revealed an energy-dependent endocytosis. However, cytotoxicity is still observed which also indicates the existence of an energy-independent pathway such as passive diffusion. This behavior has also been reported previously by Zhou *et al.* with ultra-small carbon dots with a particle size of 1–5 nm.[70] Furthermore, we have investigated the possible endocytosis process of the prepared carbon nanodots by using four different endocytosis inhibitors. Each one inhibits a specific process of the endocytosis.[71] Methyl-β-cyclodextrin (MβCD) is considered an inhibitor of lipid raft-mediated endocytosis, chlorpromazine is an inhibitor of clathrin-mediated endocytosis, genistein inhibits caveolae-mediated endocytosis, and finally amiloride is an inhibitor of micropinocytosis. These compounds at the concentrations used don't have a cytotoxicity effect on the Hep3B cells. We have found that the cytotoxicity of CNDs decreased significantly in the case of MβCD and genistein as shown in Fig. 6 which revealed that the possible CND uptake is through caveolae and lipid-mediated endocytosis. According to the literature, small nanoparticles are internalized mainly through caveolae-mediated endocytosis.[70,71] Moreover, Ji *et al.* have developed carbon nanodots from urea and citric acid and

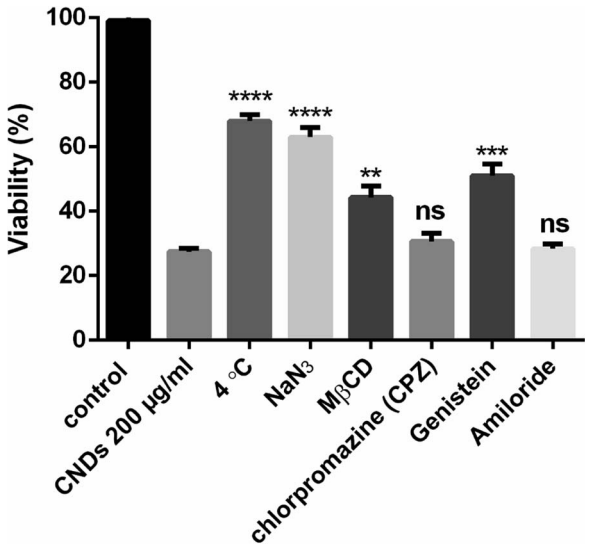

Fig. 6 Viability of Hep3B without treatment (control), after being treated with CNDs (200 μg ml^{-1}), cells incubated at 4 °C then treated with CNDs, cells incubated with NaN_3 and treated with CNDs, cells incubated with MβCD and treated with CNDs, cells incubated with CPZ and treated with CNDs, cells incubated with genistein and treated with CNDs, and finally cells incubated with amiloride and treated with CNDs. The values are expressed as mean ± SD ($n = 3$). ****$P < 0.0001$, ***$P < 0.001$, and **$P = 0.0013$, ns = not significant, compared with CNDs 200 μg ml^{-1}, using *t*-tests.

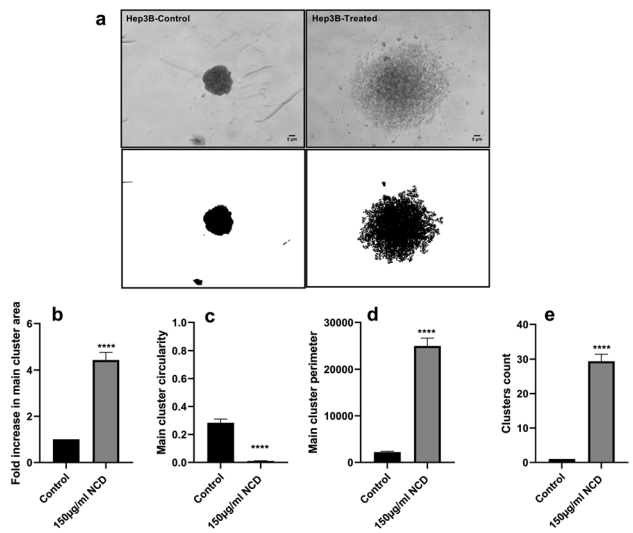

Fig. 7 Carbon nanodot blocked three-dimensional spheroid/aggregate formation. Human Hep3B liver cancer cells were tested to form spheroids without treatment (control spheroids) or in the presence of 150 μg ml^{-1} of carbon nanodots (treated spheroids) for 24 hours. (a) Images of the resulting spheroids and black-masked main clusters. Graphs of fold increase in the (b) main cluster area, (c) its circularity, and (d) its perimeter-in pixels-are presented for each condition. (e) Formed cluster count and the treated to non-treated cluster count ratio for each cell line were quantified. A cell cluster is composed of 2≥ cells. The main cluster is a spheroid under non-treated conditions and the central aggregate after dispersal under treated conditions. A circularity value of 1 designates a perfect circle. 6–8 spheroids were considered per condition. The total magnification of images is 40×. The scale bar is 5 μm.

they observed that cellular uptake is energy-dependent through lipid endocytosis and micropinocytosis.[47] In our study, the cellular uptake of our synthesized CNDs is energy-dependent and also by passive diffusion. Moreover, the main routes of endocytosis are lipid and caveolae-mediated endocytosis.

3.4. CNDs blocked 3D MCTS spheroid formation

Over the last few years, three-dimensional (3D) cultures have become an innovative tool for cellular modelling, bridging the gap between *in vitro* research and animal model studies.[72] The multicellular tumor spheroid model (MCTS) is currently coined as a 3D *in vitro* model that mimics the *in vivo* state of cancer tumors. The ability of cancer cells to group into spheroids in an *in vitro* setting indicates an enhanced tumorigenicity, resistance to chemotherapeutic drugs, and tumor-forming capacity *in vivo*.[73,74] We studied the effect of the synthesized CNDs on Hep3B cells' capacity to form spheroids. Cells were allowed to group into spheroids under non-treated conditions (Control). Importantly, treated Hep3B cells with CNDs were not able to form spheroids. Cells remained spread in small groups/clusters over a large perimeter (Fig. 7). The occupied area and perimeter of the formed cluster under treated conditions were significantly increased (Fig. 7b and d) while its circularity decreased (Fig. 7c) indicating a disordered form. The number of small clusters was significantly increased compared to the control (Fig. 7e). Altogether, these results suggest a prohibiting effect of CNDs on Hep3B cancer spheroid formation. Previous researchers have proven the relevance of hindering spheroid formation in several types of cancer notably in liver cancer with the goal of decreasing tumorigenicity and resistance to chemotherapy.[75–78]

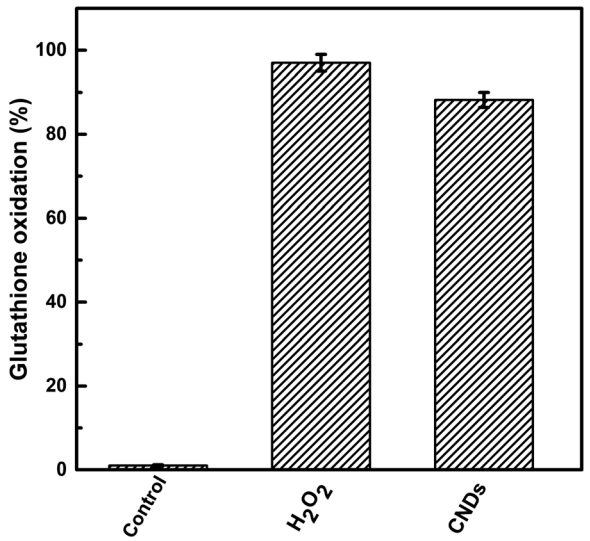

Fig. 8 Percentage of glutathione oxidation mediated by prepared CNDs. H_2O_2 was used as a positive control.

3.5. The possible mechanism of CND anticancer activity

The anticancer activity and selectivity could be referred to as the production of reactive oxygen species (ROS) by CNDs which have the responsibility to destroy many cell components such as proteins, DNA, and lipids resulting in cell death.[79] Since the membrane of cancer cells is dilapidated and weaker than that of the normal cells,[80] the CNDs select the cancer cells and kill them. The reactive oxygen species (ROS) term encompasses oxygen free radicals, such as the superoxide anion radical (O_2^-) and hydroxyl radical (OH^-), and nonradical oxidants, such as hydrogen peroxide (H_2O_2) and singlet oxygen (O_2^-).[81] Electrons (e^-) and holes (h^+) are produced upon excitation of the CNDs;

Table 1 Comparison of the cancer treatment results of our synthesized CNDs with other research utilized natural precursors

Resource	Method	Temperature (°C)	Time (h)	Size (nm)	Quantum yield (%)	Cancer cell	Inhibition concentration IC_{50} (μg ml^{-1})	Ref.
Walnut oil	Hydrothermal	220	24	10–15	14.5	MCF-7 PC-3	1.25 5	85
Cinnamon, black pepper, turmeric, and red chili	Hydrothermal	200	12	3–5	43.6	Kidney cells HK-2	2000	86
Thumbai Lour	Hydrothermal	200	5	3.8 2.9	—	Cervical cancer (HeLa)	2000 2000	87
Bamboo	Carbonization	80	2	4	2.27	Breast	2000	45
M. floribunda fruit	Hydrothermal	200	12	3.5	18	Human colon	200	88
Pineapple	Hydrothermal	120	3	2.7	9.63	Colon adenocarcinoma	2000	45
Ocimum sanctum	Hydrothermal	180	4	5	9.3	Breast	1000	89
Green tea	Carbonization	300	2	2.5–4	4.3	MCF-7 & MDA-MB-231	360	37
Glucose	Acid-assisted ultrasonic	40	4	10	6.8	Lung cells (H157)	5	90
Ginger juice	Hydrothermal	300	2	3.5–5	13.4	Hepatocellular carcinoma cell	350	68
Waste onion	Hydrothermal	120	2	7–25	28	Hela cell	1000	91
Mint	Hydrothermal	200	4	—	0.54	Breast cells	1200	38
Sage leaves	Hydrothermal	200	6	1–9	1.95	HeP3B	100	This work

therefore electrons are excited from the ground state (valence band) to the excitation state (conduction band). Several excited carriers are trapped on the CNDs because of the many surface flaws inhibiting e^- and h^+ recombination. And part of the h^+ may combine with surface-adsorbed H_2O to produce hydroxyl radicals, while the e^- may be captured by oxygen dissolved in the solution, producing superoxide radicals.[82]

To confirm the ability of the prepared CNDs to produce ROS, the percentage of glutathione oxidation was tested. Glutathione is a tripeptide that contains cysteine with a thiol group that can protect the cellular components from the damage that could be caused by ROS production.[83] Due to its abundance in cancer cells it can be used as an indicator of the cellular oxidative stress generated by carbon nanomaterials.[36,79] Herein, we utilized Ellman's assay to evaluate the percentage of glutathione activity loss (GSH%) upon incubation with the synthesized CNDs.[84] As can be observed in Fig. 8, a great fraction of the glutathione is oxidized in the presence of the CNDs (88.2%) with comparable activity to the positive control (H_2O_2). This observation confirms the high ROS production of the oxygenated CNDs which could explain their potent anticancer activity in addition to the weakness of the cancer cell membrane that permits the higher penetration of the CNDs.

Interestingly, the CNDs prepared in this work show efficient inhibition toward Hep3B cancer cells at low inhibition concentrations compared to other research studies. To the best of our knowledge this is the first time that CNDs have been synthesized from sage leaves and utilized as anticancer agents. A comparison of CNDs from different resourses and in terms of treated cancer cell lines and inhibition concentrations is presented in Table 1.

4. Conclusions

In this work, CNDs have been successfully synthesized from fresh sage leaves by a simple green hydrothermal method. Simply put, CNDs have been synthesized under mild conditions of 200 °C for 6 hours, with no addition of any chemicals and external surface passivation agent and/or further modification. CNDs have an average size of 3.6 nm; they are highly water soluble, photoluminescent, and stable with a quantum yield equal to 1.95%. Our results clearly show that CNDs have an important role in inhibiting the growth of liver cancer cells (HeP3B). The synthesized CNDs showed impressive anticancer activity at various concentrations, and the cell activity was shown to decrease with increasing concentrations from 92% at 50 μg ml^{-1} to 23% at 250 μg ml^{-1}. The normal cells (LX2) are not affected which means that the CNDs are selective for the cancer cells. The proposed anticancer mechanism is through the formation of reactive oxygen species. Interestingly, the synthesized CNDs were capable of inhibiting 3D spheroid formation indicating CNDs' potential in reducing tumorigenicity.

Author contributions

Shadi Sawalha: conceptualization, investigation, validation, visualization, supervision, and writing – original draft. Mohyeddin Assali: conceptualization, investigation, formal analysis, and writing – review & editing. Samer Abdallah: methodology, investigation, and writing – review & editing. Amal Barham, Hala Badawi, and Zeina Barham: methodology, investigation, and writing – original draft. Ahmad Ghareeb: investigation and methodology. Giuseppe Misia, Silvia Collavini, Alessandro Silvestri, and Maurizio Prato: investigation, methodology, and visualization.

Conflicts of interest

There are no conflicts to declare.

Acknowledgements

The authors acknowledge Mr Ameed Amireh from the Department of Chemistry for help in FTIR and fluorescence analysis.

Notes and references

1 T. Boobalan, M. Sethupathi, N. Sengottuvelan, P. Kumar, P. Balaji, B. Gulyás, P. Padmanabhan, S. T. Selvan and A. Arun, *ACS Appl. Nano Mater.*, 2020, **3**, 5910–5919.
2 M. Arruebo, N. Vilaboa, B. Sáez-Gutierrez, J. Lambea, A. Tres, M. Valladares and Á. González-Fernández, *Cancers*, 2011, **3**, 3279–3330.
3 D. T. Debela, S. G. Y. Muzazu, K. D. Heraro, M. T. Ndalama, B. W. Mesele, D. C. Haile, S. K. Kitui and T. Manyazewal, *SAGE Open Med.*, 2021, **9**, DOI: **10.1177/20503121211034366**.
4 M. F. Attia, N. Anton, J. Wallyn, Z. Omran and T. F. Vandamme, *J. Pharm. Pharmacol.*, 2019, **71**, 1185–1198.
5 M. Assali, N. Kittana, S. A. Qasem, R. Adas, D. Saleh, A. Arar and O. Zohud, *RSC Adv.*, 2019, **9**, 1055–1061.
6 M. Assali, A. N. Zaid, N. Kittana, D. Hamad and J. Amer, *Nanotechnology*, 2018, **29**, 245101.
7 M. Assali, N. Kittana, S. Dayyeh and N. Khiar, *Nanotechnology*, 2021, **32**, 205101.
8 M. Assali, N. Kittana, I. Badran and S. Omari, *RSC Adv.*, 2023, **13**, 7000–7008.
9 Q. Jia, Z. Zhao, K. Liang, F. Nan, Y. Li, J. Wang, J. Ge and P. Wang, *Mater. Chem. Front.*, 2020, **4**, 449–471.
10 C.-L. Shen, H.-R. Liu, Q. Lou, F. Wang, K.-K. Liu, L. Dong and C.-X. Shan, *Theranostics*, 2022, **12**, 2860–2893.
11 G. Nocito, G. Calabrese, S. Forte, S. Petralia, C. Puglisi, M. Campolo, E. Esposito and S. Conoci, *Cancers*, 2021, **13**, 1991.
12 M.-H. Chan, B.-G. Chen, L. T. Ngo, W.-T. Huang, C.-H. Li, R.-S. Liu and M. Hsiao, *Pharmaceutics*, 2021, **13**, 1874.
13 X. Xu, R. Ray, Y. Gu, H. J. Ploehn, L. Gearheart, K. Raker and W. A. Scrivens, *J. Am. Chem. Soc.*, 2004, **126**, 12736–12737.
14 N. Papaioannou, A. Marinovic, N. Yoshizawa, A. E. Goode, M. Fay, A. Khlobystov, M.-M. Titirici and A. Sapelkin, *Sci. Rep.*, 2018, **8**, 6559.
15 S. Anwar, H. Ding, M. Xu, X. Hu, Z. Li, J. Wang, L. Liu, L. Jiang, D. Wang, C. Dong, M. Yan, Q. Wang and H. Bi, *ACS Appl. Bio Mater.*, 2019, **2**, 2317–2338.

16 D. Tan, Y. Yamada, S. Zhou, Y. Shimotsuma, K. Miura and J. Qiu, *Carbon*, 2014, **69**, 638–640.
17 A. Szabó, C. Perri, A. Csató, G. Giordano, D. Vuono and J. B. Nagy, *Materials*, 2010, **3**, 3092–3140.
18 S. Sawalha, M. Assali, A. Nasasrah, M. Salman, M. Nasasrah, M. Jitan, H. S. Hilal and A. Zyuod, *RSC Adv.*, 2022, **12**, 4490–4500.
19 S. Sawalha, R. Hamed and M. Assali, *ChemistrySelect*, 2023, **8**, e202300522.
20 R. Hamed, S. Sawalha, M. Assali, R. A. Shqair, A. Al-Qadi, A. Hussein, R. Alkowni and S. Jodeh, *Surf. Interfaces*, 2023, **38**, 102760.
21 Indriyati, M. M. Munir, M. Nasir and F. Iskandar, *IOP Conf. Ser.: Earth Environ. Sci.*, 2022, **1017**, 012009.
22 M. Behi, L. Gholami, S. Naficy, S. Palomba and F. Dehghani, *Nanoscale Adv.*, 2022, **4**, 353–376.
23 V. S. Sivasankarapillai, A. Vishnu Kirthi, M. Akksadha, S. Indu, U. Dhiviya Dharshini, J. Pushpamalar and L. Karthik, *Nanoscale Adv.*, 2020, **2**, 1760–1773.
24 N. K. Quang, N. N. Hieu, V. V. Q. Bao, V. T. Phuoc, L. X. D. Ngoc, L. Q. Doc, N. M. Tri, L. V. T. Son, L. V. T. Son and C. T. C. Ha, *New Carbon Mater.*, 2022, **37**, 595–602.
25 A. V. Longo, A. Sciortino, M. Cannas and F. Messina, *Phys. Chem. Chem. Phys.*, 2020, **22**, 13398–13407.
26 M. Aslan and H. Eskalen, *Fullerenes, Nanotubes Carbon Nanostruct.*, 2021, **29**, 1026–1033.
27 D. S. Chauhan, M. A. Quraishi and C. Verma, *Carbon Lett.*, 2022, **32**, 1603–1629.
28 J. Lan, C. Liu, M. Gao and C. Huang, *Talanta*, 2015, **144**, 93–97.
29 T. Ghosh, R. Ghosh, U. Basak, S. Majumdar, R. Ball, D. Mandal, A. K. Nandi and D. P. Chatterjee, *J. Mater. Chem. A*, 2018, **6**, 6476–6492.
30 J. Schneider, C. J. Reckmeier, Y. Xiong, M. von Seckendorff, A. S. Susha, P. Kasák and A. L. Rogach, *J. Phys. Chem. C*, 2017, **121**, 2014–2022.
31 X. Dong, Y. Su, H. Geng, Z. Li, C. Yang, X. Li and Y. Zhang, *J. Mater. Chem. C*, 2014, **2**, 7477–7481.
32 B. De and N. Karak, *RSC Adv.*, 2013, **3**, 8286–8290.
33 Y. Liu, Y. Zhao and Y. Zhang, *Sens. Actuators, B*, 2014, **196**, 647–652.
34 M. Xue, Z. Zhan, M. Zou, L. Zhang and S. Zhao, *New J. Chem.*, 2016, **40**, 1698–1703.
35 Isnaeni, I. Rahmawati, R. Intan and M. Zakaria, *J. Phys.: Conf. Ser.*, 2018, **985**, 012004.
36 S. Sawalha, M. Assali, M. Raddad, T. Ghneem, T. Sawalhi, M. Almasri, A. Zarour, G. Misia, M. Prato and A. Silvestri, *ACS Appl. Bio Mater.*, 2022, **5**, 4860–4872.
37 P.-C. Hsu, P.-C. Chen, C.-M. Ou, H.-Y. Chang and H.-T. Chang, *J. Mater. Chem. B*, 2013, **1**, 1774–1781.
38 S. Shahid, S. Mohiyuddin and G. Packirisamy, *J. Nanosci. Nanotechnol.*, 2020, **20**, 6305–6316.
39 B. Chen, F. Li, S. Li, W. Weng, H. Guo, T. Guo, X. Zhang, Y. Chen, T. Huang, X. Hong, S. You, Y. Lin, K. Zeng and S. Chen, *Nanoscale*, 2013, **5**, 1967–1971.
40 L. Xiao and H. Sun, *Nanoscale Horiz.*, 2018, **3**, 565–597.
41 X. Zhang, X. He, Y. Li, Z. Zhang, Y. Ma, F. Li and J. Liu, *J. Nanosci. Nanotechnol.*, 2013, **13**, 5254–5259.
42 P. Jayasekhar Babu, S. Saranya, Y. D. Singh, M. Venkataswamy, A. M. Raichur and M. Doble, *Opt. Mater.*, 2021, **117**, 111120.
43 A. A. Kokorina, E. S. Prikhozhdenko, N. V. Tarakina, A. V. Sapelkin, G. B. Sukhorukov and I. Y. Goryacheva, *Carbon*, 2018, **127**, 541–547.
44 M. Righetto, F. Carraro, A. Privitera, G. Marafon, A. Moretto and C. Ferrante, *J. Phys. Chem. C*, 2020, **124**, 22314–22320.
45 Y.-Y. Chen, W.-P. Jiang, H.-L. Chen, H.-C. Huang, G.-J. Huang, H.-M. Chiang, C.-C. Chang, C.-L. Huang and T.-Y. Juang, *RSC Adv.*, 2021, **11**, 16661–16674.
46 C.-L. Li, C.-M. Ou, C.-C. Huang, W.-C. Wu, Y.-P. Chen, T.-E. Lin, L.-C. Ho, C.-W. Wang, C.-C. Shih, H.-C. Zhou, Y.-C. Lee, W.-F. Tzeng, T.-J. Chiou, S.-T. Chu, J. Cang and H.-T. Chang, *J. Mater. Chem. B*, 2014, **2**, 4564–4571.
47 Z. Ji, Z. Yin, Z. Jia and J. Wei, *Langmuir*, 2020, **36**, 8632–8640.
48 D. Vercauteren, R. E. Vandenbroucke, A. T. Jones, J. Rejman, J. Demeester, S. C. De Smedt, N. N. Sanders and K. Braeckmans, *Mol. Ther.*, 2010, **18**, 561–569.
49 G. Privitera, T. Luca, S. Castorina, R. Passanisi, G. Ruberto and E. Napoli, *Asian Pac. J. Trop. Biomed.*, 2019, **9**, 24–28.
50 S. Sahu, B. Behera, T. K. Maiti and S. Mohapatra, *Chem. Commun.*, 2012, **48**, 8835–8837.
51 B. R. Al-Hashimi, K. M. Omer, H. S. Rahman and H. H. Othman, *Spectrochim. Acta, Part A*, 2021, **244**, 118835.
52 P. Das, M. Bose, S. Ganguly, S. Mondal, A. K. Das, S. Banerjee and N. C. Das, *Nanotechnology*, 2017, **28**, 195501.
53 K. Radhakrishnan, P. Panneerselvam and M. Marieeswaran, *Anal. Methods*, 2019, **11**, 490–506.
54 Y. Xu, C.-J. Tang, H. Huang, C.-Q. Sun, Y.-K. Zhang, Q.-F. Ye and A.-J. Wang, *Chin. J. Anal. Chem.*, 2014, **42**, 1252–1258.
55 P. Roy, P.-C. Chen, A. P. Periasamy, Y.-N. Chen and H.-T. Chang, *Mater. Today*, 2015, **18**, 447–458.
56 Y. Ding, F. Zhang, J. Xu, Y. Miao, Y. Yang, X. Liu and B. Xu, *RSC Adv.*, 2017, **7**, 28754–28762.
57 H. Li, S. Han, B. Lyu, T. Hong, S. Zhi, L. Xu, F. Xue, L. Sai, J. Yang, X. Wang and B. He, *Chin. Chem. Lett.*, 2021, **32**, 2887–2892.
58 C. Dhanush and M. G. Sethuraman, *Spectrochim. Acta, Part A*, 2021, **260**, 119920.
59 K. K. Karali, L. Sygellou and C. D. Stalikas, *Talanta*, 2018, **189**, 480–488.
60 H. Sutanto, I. Alkian, N. Romanda, I. W. L. Lewa, I. Marhaendrajaya and P. Triadyaksa, *AIP Adv.*, 2020, **10**, 055008.
61 H. Shabbir, T. Tokarski, D. Ungor and M. Wojnicki, *Materials*, 2021, **14**, 7604.
62 M. Amjad, M. Iqbal, A. Faisal, A. M. Junjua, I. Hussain, S. Z. Hussain, H. A. Ghramh, K. A. Khan and H. A. Janjua, *Nanoscale Adv.*, 2019, **1**, 2924–2936.
63 Y. Liu, Y. Zhao and Y. Zhang, *Sens. Actuators, B*, 2014, **196**, 647–652.
64 K. M. Omer, K. H. Hama Aziz and S. J. Mohammed, *New J. Chem.*, 2019, **43**, 12979–12986.

65 T. G. Chatzimitakos, A. I. Kasouni, A. N. Troganis and C. D. Stalikas, *ACS Appl. Mater. Interfaces*, 2018, **10**, 16024–16032.
66 A. Sharma, T. Gadly, A. Gupta, A. Ballal, S. K. Ghosh and M. Kumbhakar, *J. Phys. Chem. Lett.*, 2016, **7**, 3695–3702.
67 H. Ding, X.-H. Li, X.-B. Chen, J.-S. Wei, X.-B. Li and H.-M. Xiong, *J. Appl. Phys.*, 2020, **127**, 231101.
68 R.-J. Fan, Q. Sun, L. Zhang, Y. Zhang and A.-H. Lu, *Carbon*, 2014, **71**, 87–93.
69 P. Foroozandeh and A. A. Aziz, *Nanoscale Res. Lett.*, 2018, **13**, 339.
70 N. Zhou, S. Zhu, S. Maharjan, Z. Hao, Y. Song, X. Zhao, Y. Jiang, B. Yang and L. Lu, *RSC Adv.*, 2014, **4**, 62086–62095.
71 S. Behzadi, V. Serpooshan, W. Tao, M. A. Hamaly, M. Y. Alkawareek, E. C. Dreaden, D. Brown, A. M. Alkilany, O. C. Farokhzad and M. Mahmoudi, *Chem. Soc. Rev.*, 2017, **46**, 4218–4244.
72 A. G. Mitrakas, A. Tsolou, S. Didaskalou, L. Karkaletsou, C. Efstathiou, E. Eftalitsidis, K. Marmanis and M. Koffa, *Int. J. Mol. Sci.*, 2023, **24**, 6949.
73 R. B. Mokhtari, B. Qorri, M. Sambi, N. Baluch, S. Kumar, B. Das, M. R. Szewczuk, H. Yeger and H.-L. M. Cheng, *Cancers*, 2021, **13**, 2784.
74 B. Pinto, A. C. Henriques, P. M. A. Silva and H. Bousbaa, *Pharmaceutics*, 2020, **12**, 1186.
75 H. Lu, L. Noorani, Y. Jiang, A. W. Du and M. H. Stenzel, *J. Mater. Chem. B*, 2017, **5**, 9591–9599.
76 A. Wang, L. A. Madden and V. N. Paunov, *J. Mater. Chem. B*, 2020, **8**, 10487–10501.
77 D. Melnik, C. Sahana, N. Kopp, I. Wehland, D. Grimm and M. Krüger, *Cells*, 2020, **9**, 367.
78 M. Hawash, M. T. Qaoud, N. Jaradat, S. Abdallah, S. Issa, N. Adnan, M. Hoshya, S. Sobuh and Z. Hawash, *Biomimetics*, 2022, **7**, 247.
79 M. Assali, M. Almasri, N. Kittana and D. Alsouqi, *ACS Biomater. Sci. Eng.*, 2019, **6**, 112–121.
80 C. Alibert, B. Goud and J.-B. Manneville, *Biol. Cell*, 2017, **109**, 167–189.
81 M. Schieber and N. S. Chandel, *Curr. Biol.*, 2014, **24**, R453–R462.
82 S. Prasad, P. Shanmugam, K. Bhuvaneswari, G. Palanisamy, T. Pazhanivel, T. Arunkumar, M. S. AlSalhi and M. J. Aljaafreh, *Crystals*, 2020, **10**, 300.
83 A. Pompella, A. Visvikis, A. Paolicchi, V. D. Tata and A. F. Casini, *Biochem. Pharmacol.*, 2003, **66**, 1499–1503.
84 G. L. Ellman, *Arch. Biochem. Biophys.*, 1959, **82**, 70–77.
85 E. Arkan, A. Barati, M. Rahmanpanah, L. Hosseinzadeh, S. Moradi and M. Hajialyani, *Adv. Pharm. Bull.*, 2018, **8**, 149–155.
86 N. Vasimalai, V. Vilas-Boas, J. Gallo, M. d. F. Cerqueira, M. Menéndez-Miranda, J. M. Costa-Fernández, L. Diéguez, B. Espiña and M. T. Fernández-Argüelles, *Beilstein J. Nanotechnol.*, 2018, **9**, 530–544.
87 P. T. Varsha Raveendran and N. K. Renuka, *Mater. Chem. Phys.*, 2022, **288**, 126236.
88 R. Atchudan, T. N. J. I. Edison, S. Perumal, N. Muthuchamy and Y. R. Lee, *J. Photochem. Photobiol., A*, 2020, **390**, 112336.
89 A. Kumar, A. R. Chowdhuri, D. Laha, T. K. Mahto, P. Karmakar and S. K. Sahu, *Sens. Actuators, B*, 2017, **242**, 679–686.
90 M. Ajmal, U. Yunus, A. Matin and N. U. Haq, *J. Photochem. Photobiol., B*, 2015, **153**, 111–120.
91 R. Bandi, B. R. Gangapuram, R. Dadigala, R. Eslavath, S. S. Singh and V. Guttena, *RSC Adv.*, 2016, **6**, 28633–28639.